Surface & Coatings Technology 220 (2013) 244–247

Contents lists available at SciVerse ScienceDirect

Surface & Coatings Technology

journal homepage: www.elsevier.com/locate/surfcoat

Definition of brightness temperature and restoration of true temperature in laser cladding using infrared camera

M. Doubenskaia [a,*], M. Pavlov [b], S. Grigoriev [b], I. Smurov [a]

[a] Université de Lyon, Ecole Nationale d'Ingénieurs de Saint-Etienne (ENISE), DIPI Laboratory, 58 rue Jean Parot, 42023, Saint-Etienne Cedex 2, France
[b] Moscow State Technological University "Stankin", Vadkovsky per. 1, 127994 Moscow, Russia

ARTICLE INFO

Available online 27 October 2012

Keywords:
Laser cladding
Infrared camera
Brightness temperature
Temperature restoration
Cooling rate

ABSTRACT

Laser cladding is a surface engineering technique allowing depositing material of a different nature in the form of a powder or a wire on the surface of a metallic part.
In this study, the laser cladding technique was used to deposit TiAl6V4 coating on TiAl6V4 substrate to study repairing of worn parts. An infrared camera was applied to measure radiation emission field that was transformed into brightness temperature after camera calibration by a black body. The emissivity value was found using known temperature of liquid–solid transition. True temperature profiles in cladded bead, temperature evolution at liquid–solid transition and cooling rates were found using gray body assumption.

1. Introduction

The laser cladding (LC) is an effective method for repairing worn components and enhancing surface properties such as wear or corrosion resistance. Also it is used for near net shape manufacturing of metallic parts [1–3]. The main advantage of LC in comparison to Thermal Spray is the metallurgical contact between coating and substrate. The disadvantages are related to relatively low productivity (1.5–3 kg/h of powder feeding) and large heat affected zone (HAZ) that limits LC application to the parts of relatively big size.

There is an evident interest to know and to control temperature distribution in LC in order to avoid thermal decomposition of complex powder blends, and to minimize dilution, residual stresses and cracking. Several different methods and experimental set-up were applied, to reach the goal: A compact LC head with integrated sensors and coaxial powder feeding was developed and qualified for industrial applications [4]. The process monitoring and control based on the infrared temperature signal were adopted in order to ensure product quality and reproducibility. The utilization of a raw signal requires application of recalibration procedure when process parameters are modified or one powder is replaced by another one.

Alternative approach is to combine signals from CCD camera with temperature measurements by a pyrometer [5]. The melt pool height is monitored by three high-speed charged couple device cameras in a triangulation setup. The melt pool temperature is monitored by a single spot bi-color pyrometer. Even this complicated set-up cannot provide temperature distribution in the molten pool and HAZ.

To solve the problem of temperature measurements several originally developed pyrometers were used to study CO_2 and Nd:YAG LC [6,7]. Brightness temperature in spot and brightness temperature profiles were measured versus modification of basic cladding parameters as laser power, scanning speed, and powder feeding rate. Single spot multi-wavelength pyrometer was applied for true temperature restoration in pulsed-periodic Nd:YAG laser cladding, but temperature distribution was not found.

Modern infrared cameras with advanced performance can provide much more detailed spatial and temporal signals than pyrometers but they are mainly used for process visualization because of nonlinear response on the incoming radiation in a wide spectral and temperature range that makes calibration procedure questionable. For example, infrared camera was used for visualization of thermal phenomena in CO_2 laser cladding, but neither brightness nor true temperature was restored [8].

2. Experimental facilities and materials

CW Nd:YAG laser TRUMPF HL4006D with coaxial cladding head YC 50 by Precitec and MEDICOAT powder feeder was used. Argon as protective gas (flow rate 6 l/min) and powder carrier gas (flow rate 6 and 9 l/min) was applied.

Experiments were carried out with a scanning speed of $S = 1$ mm/s, a laser power of $P = 500$ and 750 W, and a powder feeding rate of $F = 10.5$ g/min. Distance from nozzle to substrate was 9 and 10 mm.

Spatial energy distribution in laser beam was measured by Laserscope UFF 100.

TiAl6V4, +50–100 μm (measured by optical granulo-morphometer ALPAGA 500 NANO) powder fabricated by TLS Technik GmbH & Co (Bitterfeld, Germany) was used in LC.

* Corresponding author. Tel.: +33 477437565; fax: +33 477743497.
E-mail address: maria.doubenskaia@enise.fr (M. Doubenskaia).

0257-8972/$ – see front matter © 2012 Elsevier B.V. All rights reserved.
http://dx.doi.org/10.1016/j.surfcoat.2012.10.044

Spatial distribution of emitted thermal radiation from laser cladded bead was acquired by infrared camera FLIR Phoenix RDAS™. The camera is equipped by an InSb sensor with 3 to 5 μm band pass arranged on 320×256 pixel array. The brightness temperature measurements were realized under the following conditions: exposition time of 10 μs, observation zone of 15×10 mm^2, and angle of observation of 40° relative to the surface normal. The infrared camera was fixed with laser cladding head (Fig. 1).

3. Method of brightness temperature definition and true temperature restoration

Infrared camera calibration using black body model MICRON M390 was carried out to transform raw signal to brightness temperature: Raw signals from camera were written with 50 °C step from 600 °C to 1300 °C. At the black body temperature 1300 °C raw signal has reached 7100 a.u., which exceeds the maximum value of experimental signals.

To verify the infrared photo detector response on the variation of incoming radiation, the energy density flux in the 3–5 μm spectral range (i.e. the camera spectral range) was calculated using Plank's law for the temperature range used for camera calibration. Then the camera signal in a.u. was plotted versus energy density flux. It was found that the resulting curve is well approximated by a linear function. It means that the infrared photo detector is characterized by linear response on the incoming radiation.

The effect of temperature stabilization all over the molten pool surface during liquid–solid phase transition was found for three different sets of cladding conditions. The level of signal in a.u. is exactly the same. It was supposed that this value corresponds to the liquid–solid phase transition of TiAl6V4. In this way the emissivity value, $\varepsilon = 0.201$, at the phase transition was found. For the true temperature restoration in the full temperature range, the gray body hypothesis, i.e. $\varepsilon = \text{const}$, in the 3–5 μm spectral range was applied. The eventual variation of emissivity with temperature was neglected. It is known that Ti emissivity in the 20–900 °C temperature range represents the similar value and it slightly depends on temperature [9,10].

4. Results and discussion

The thermal image of cladding zone registered by infrared camera is presented in Fig. 2. It is characterized by non-monotonous ring-shape spatial distribution of emitted thermal radiation. The central maximum is explained by the maximum of energy density flux of the laser beam with pseudo-Gaussian shape that results in higher temperature at beam axis. The ring-shape zone with high thermal emission corresponds to the peripheral area of the molten pool, where oxides and other nonmetallic inclusions are usually concentrated under the action of thermocapillary convection, and also to the neighboring solid phase areas. This is confirmed by visual observation of cladded bead surface and substrate. It is known that non-metallic inclusions and oxides are characterized by higher emissivity than metals at the same temperature. This is the reason of higher thermal emission from the molten pool boundaries and oxidized zones of the substrate.

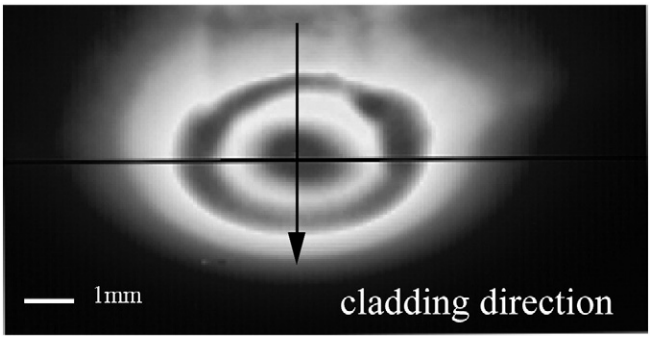

Fig. 2. False-color picture representing infrared image of melt pool and HAZ registered by infrared camera FLIR Phoenix RDAS™ in 3–5 μm spectral range. Laser power $P = 750$ W, scanning speed $S = 1$ mm/s, powder feeding rate $F = 10.5$ g/min, flow rate of powder carrier gas $f = 9$ l/min, and cladding nozzle–substrate distance is 10 mm.

This is confirmed by evolution of radiation emission profiles at the cooling stage, i.e. after the end of laser irradiation (Fig. 3): The peripheral extremes exist after the end of laser action and even after the end of solidification. If they are related to real temperature extremes then temperature gradients should be so strong that resulting heat flux will modify temperature distribution, in particular in their neighborhood, and strongly decrease temperature spikes. It is known that nonmonotonous distribution of surface temperature, as the result of nonmonotonous laser beam profile, could exist during laser action but never after its end when high thermal conductivity of metals and surface heat losses quickly equalizes surface temperature values [11,12].

The evolution of emission profiles in the central part of cladded bead during the cooling stage is characterized by a quick disappearance of temperature maximum and temperature stabilization at the constant value, that corresponds to the liquid–solid phase transition of TiAl6V4. Further on, solidification starts from the periphery of the molten pool and completely transforms it into solid phase. The qualitatively similar evolution of surface temperature was obtained by

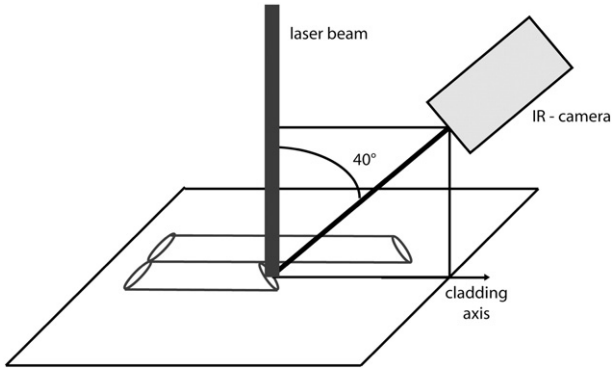

Fig. 1. Schema of temperature measurements.

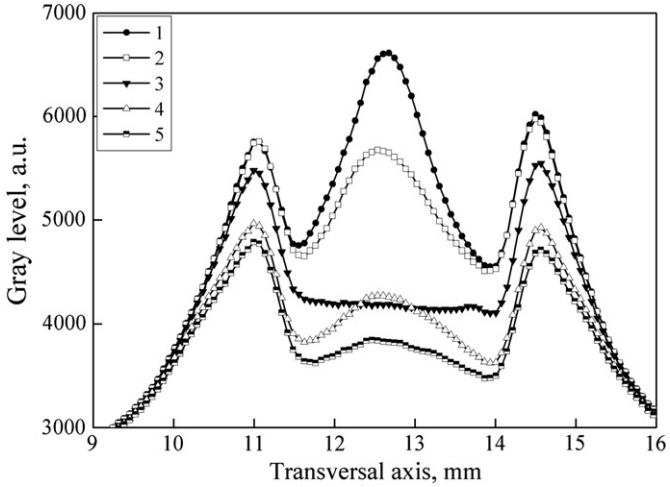

Fig. 3. Evolution of transversal profiles of thermal emission along the strait line shown in Fig. 1 at the end of laser cladding and after laser cut-off at $t = 0$. Laser power $P = 750$ W, scanning speed $S = 1$ mm/s, powder feeding rate $F = 10.5$ g/min, flow rate of powder carrier gas $f = 9$ l/mi, and cladding nozzle–substrate distance is 10 mm. Curve $1 - t = 0$ ms; $2 - t = 8$ ms; $3 - t = 33$ ms; $4 - t = 74$ ms; and $5 - t = 98$ ms.

numerical simulation analyzing melting–solidification transition in laser action on metal slabs [11].

Under the assumption that the value of temperature stabilization at solidification corresponds to the known melting point of TiAl6V4 which is equal to 1660 °C under the equilibrium conditions, it is possible to define the emissivity value that in the present case equals to $\varepsilon = 0.201$.

It was shown that laser power is one of the main governing parameters in LC [1–3]. Its influence on surface distribution of brightness temperature is presented in Fig. 4. The increase of track width and HAZ size with laser power is evident.

The transversal profiles of true temperature (Fig. 5) have near Gaussian spatial distribution that corresponds to the one of the laser beam. The maximum temperature values, that are about 2700 °C, well exceed the melting point of TiAl6V4. High temperature gradients at melt surface, in particular in the zone of laser irradiation, provoke thermocapillary convection that transports melt from the zones with higher temperature towards the ones with lower temperature. For the temperature profiles presented in Fig. 5, and linear decrease of surface tension with temperature, that is typical for metals, the melt on the surface moves from the center towards peripheral regions of the molten pool [2,3,11]. This corresponds well to the fact that oxides are collected mainly in these regions.

The evolution of surface temperature in the middle of the laser irradiation zone before and after the end of cladding is presented in Fig. 6(a). Three distinct stages of cooling are as following: (a) cooling of liquid phase that is characterized by rapid temperature decrease; (b) liquid–solid phase transition in the near surface area that is characterized by nearly constant temperature; and (c) cooling of solid phase that is characterized by further temperature decrease but less rapid than during stage (a). The quasi-constant value of temperature at liquid–solid phase transition that is sometimes called "solidification shelf" is close to the value of liquid–solid phase transition for TiAl6V4 that is equal to 1660 °C under the equilibrium conditions.

The corresponding cooling rates are presented in Fig. 6(b). The extreme value of cooling rate reaches 60 kK/s during melt cooling, later on the cooling rate is close to zero during liquid–solid phase transition, and finally there exists the second extreme value equals to 10 kK/s during solid phase cooling. The difference of the extreme values of cooling rate is explained by the different values of corresponding temperature gradients, the highest one corresponds to the initial stage of melt cooling. Indeed, the maximum value of temperature gradient corresponds to the period of laser action, that in a near surface layer could be estimated as $dT/dx \sim -q/\lambda$, where q is energy density flux, λ is thermal conductivity [12]. After the end of laser action, thermal conductivity towards the bulk material as well as surface heat losses quickly decreases temperature gradient. The qualitatively similar results were obtained by numerical simulation of phase transitions in pulsed laser action on metallic slabs [13].

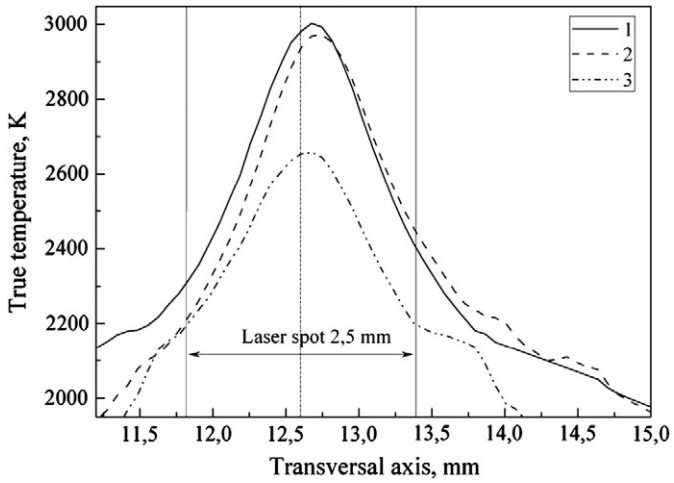

Fig. 5. Transversal profiles of true temperature in the molten pool during laser cladding restored using $\varepsilon = 0.201$ value and gray body hypothesis. Parameters: *1* — $P = 500$ W; $f = 6$ l/min; cladding nozzle–substrate distance is 10 mm; *2* — $P = 750$ W; $f = 9$ l/min; cladding nozzle–substrate distance is 10 mm; and *3* — $P = 750$ W; $f = 9$ l/min; cladding nozzle–substrate distance is 9 mm. Scanning speed $S = 1$ mm/s, and powder feeding rate $F = 10.5$ g/min.

5. Conclusion

The raw signal registered by infrared camera was transformed into brightness temperature using calibration with a black body. Surface distribution of brightness temperature in laser cladding zone was found. Emissivity was calculated by comparison of brightness temperature at the liquid–solid transition with the known melting point. True temperature profiles in the molten pool were restored from brightness temperature and known emissivity value by application of gray body hypothesis. True temperature evolution in the melt pool and cooling rates of the liquid and solid phases were found.

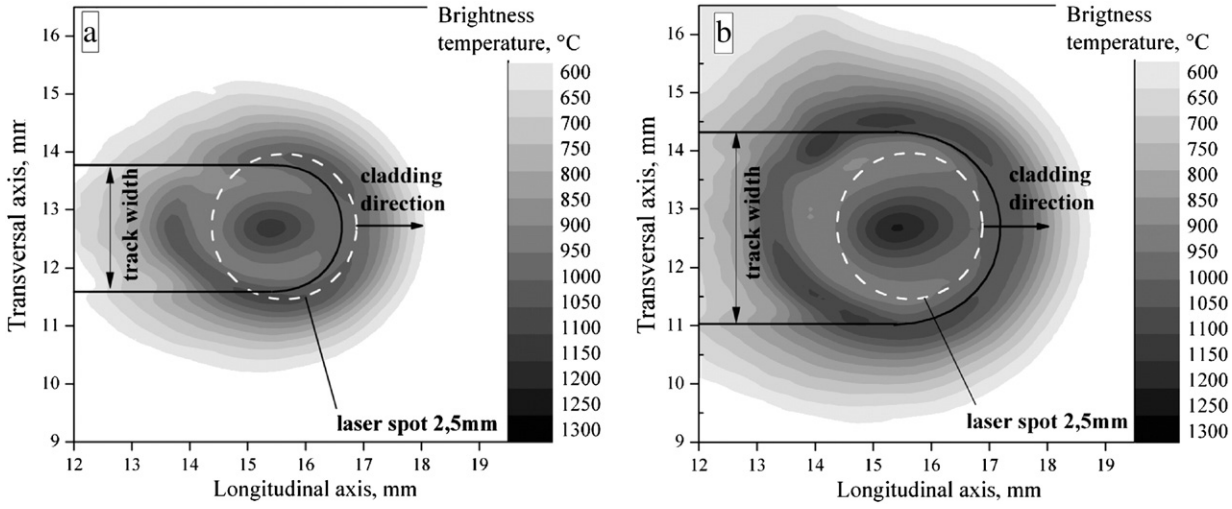

Fig. 4. Brightness temperature distribution in the cladded zone obtained by calibration of infrared camera with the black-body. Scanning speed $S = 1$ mm/s, laser spot size $d = 2.5$ mm, and powder feeding rate $F = 10.5$ g/min. (a) $P = 500$ W, $f = 6$ l/min and (b) $P = 750$ W, $f = 9$ l/min.

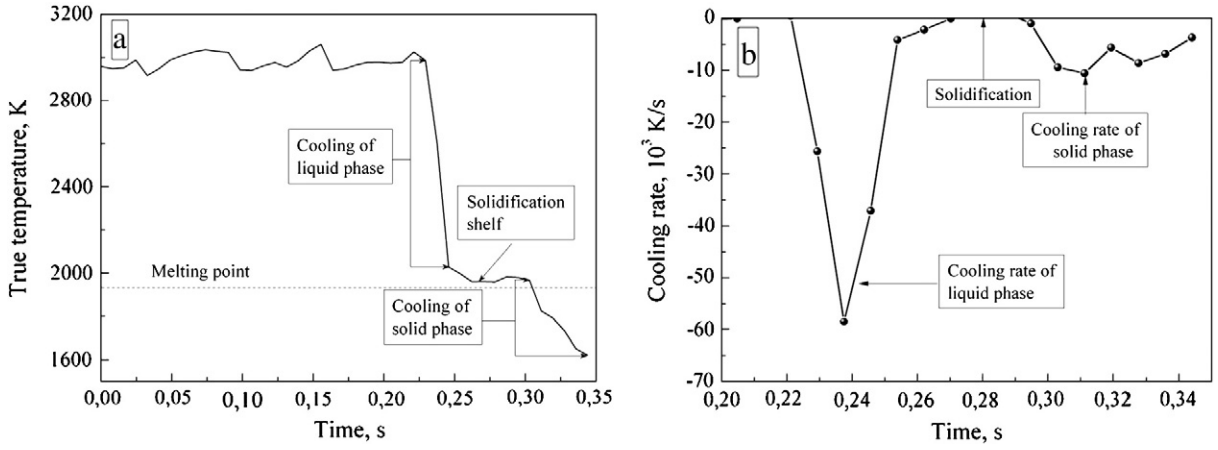

Fig. 6. (a) Evolution of true temperature in the center of molten pool at the end of cladding; and (b) cooling rates in the center of the molten pool after laser shut-down. Parameters: $P=750$ W; $f=9$ l/min, $S=1$ mm/s, $F=10.5$ g/min, and cladding nozzle–substrate distance is 10 mm.

Acknowledgment

The study was supported by the grant of the Government of Russian Federation (decree N220).

References

[1] John C. Ion, Laser Processing of Engineering Materials: Principles, Procedure and Industrial Application, 1st ed. Elsevier Butterworth-Heinemann, Burlington, MA, 2005.
[2] E. Toyserkani, A. Khajepour, S. Corbin, Laser cladding, CRS Press, Boca Raton, Florida, 2005.
[3] G. Gladush, I. Smurov, Physics of Laser Materials Processing: Theory and Experiment, 1st ed. Springer, 2011.
[4] G. Bi, B. Schürmann, A. Gasser, K. Wissenbach, R. Poprawe, Int. J. Mach. Tools Manuf. 47 (2007) 555.
[5] L. Song, V. Bagavath-Singh, B. Dutta, J. Mazumder, Int. J. Adv. Manuf. Technol. 58 (2012) 247.
[6] M. Doubenskaya, Ph. Bertrand, I. Smurov, Thin Solid Films 453-454C (2003) 477.
[7] M. Doubenskaia, Ph. Bertrand, I. Smurov, Surf. Coat.Technol. 25 (2006) 1955.
[8] M. Doubenskaia, F. Bayle, I. Smurov, D. Novichenko, in: A. Ostendof, T. Graf, D. Petring, A. Otto (Eds.), Lasers in Manufacturing, WLT, Munich, 2009, p. 591.
[9] In: D.E. Gray (Ed.), American Institute of Physics Handbook, 3rd. ed., McGraw-Hill, New-York, 1972.
[10] J. Yang, S. Sun, M. Brandt, W. Yan, J. Mater. Proc. Technol. 210 (2010) 2215.
[11] I. Smurov, M. Ignatiev, in: J. Mazumder, O. Conde, R. Villar, W. Steen (Eds.), Laser Processing: Surface Treatment and Film Deposition, NATO ASI Series, Series E: Applied Sciences, vol. 307, Kluwer Academic Publishers, The Netherlands, 1996, p. 267.
[12] N. Rykalin, A. Uglov, I. Zuev, A. Kokora, Laser and Electron Beam Material Processing, Mir Publisher, Moscow, 1988.
[13] I. Smurov, A. Lashin, in: S. Martellucci, A.N. Chester, A.M. Scheggi (Eds.), Laser Applications in Mechanical Industry, NATO ASI Series, Series E: Applied Science, vol. 238, Kluwer Academic Publishers, Dordrecht, 1993, p. 165.